Dynamics of gate-controlled superconducting Dayem bridges

N.B. When citing this work, cite the original published paper.

(article starts on next page)

Dynamics of gate-controlled superconducting Dayem bridges ⊕

François Joint ✉ ⓘ ; Kazi Rafsanjani Amin; Ivo P. C. Cools ⓘ ; Simone Gasparinetti ⓘ

Check for updates

View Online

Export Citation

AIP Publishing

Dynamics of gate-controlled superconducting Dayem bridges (EP)

François Joint,[1,2,a] (iD) Kazi Rafsanjani Amin,[1] Ivo P. C. Cools,[1] (iD) and Simone Gasparinetti[1] (iD)

AFFILIATIONS

[1]Department of Microtechnology and Nanoscience, Chalmers University of Technology, 412 96 Gothenburg, Sweden

[2]Group for Advanced Receiver Development (GARD), Department of Space, Earth, and Environment,
  Chalmers University of Technology, Gothenburg, 412 96 Sweden

[a]Author to whom correspondence should be addressed: joint@chalmers.se

ABSTRACT

Local control of superconducting circuits by high-impedance electrical gates offers potential advantages in superconducting logic, quantum processing units, and cryoelectronics. Recent experiments have reported gate-controlled supercurrent in Dayem bridges made of metallic superconductors, mediated by direct current leakage, out-of-equilibrium phonons, or possibly other mechanisms. However, a time-domain characterization of this effect has been lacking. Here, we integrate Dayem bridges made of niobium on silicon into coplanar waveguide resonators and measure the effect of the gate voltage at steady state and during pulsed operation. We consider two types of arrangements for the gate: a side-coupled gate and a remote injector. In both cases, we observe sizable changes in the real and the imaginary part of the constriction's impedance for gate voltages of the order of 1 V. However, we find striking differences in the time-domain dynamics, with the remote injector providing a faster and more controlled response. Our results contribute to our understanding of gate-controlled superconducting devices and their suitability for applications.

In recent years, the potential of voltage-controlled superconducting logic has garnered significant attention due to its promising integration with complementary metal–oxide–semiconductor (CMOS)[1] technologies and potential superiority over rapid single flux quantum (RSFQ) logic. Numerous studies[2–7] have demonstrated reversible switching of a superconducting nanowire (NW) between the superconducting and normal (metallic) states by applying a gate voltage (V_G). However, the microscopic mechanism responsible for this effect remains unclear and highly debated.[4,8,9] Given the wide range of superconductors, substrates, fabrication processes, and characterization techniques employed across the studies, it has been suggested that various mechanisms may contribute to the effect.[10]

Most studies of gate-controlled superconductivity focused on dc measurements of the switching current of the nanowire under varying gate voltage and magnetic field. In a few studies,[5,8,11] the complex impedance of the nanowire at microwave frequencies has been probed by embedding the nanowire in a coplanar waveguide (CPW) resonator coupled to a feedline. In these studies, it was found that for increasing gate voltage, the kinetic inductance of the nanowires increases, resulting in a decrease in the resonator's frequency, and, at the same time,

dissipation in the circuit also increases, resulting in a decrease in the resonator's quality factor.

Notwithstanding these studies, little is known about the response of gate-tunable superconducting nanowires to a time-dependent gate voltage. In Ref. 4, a switching time of 100 ns was reported for gated TiN nanowires on Si, but this figure was limited by the low-frequency setup used in the measurements. More comprehensive time-domain studies are thus needed. On the one hand, time-domain studies provide additional information that may help elucidate the microscopic mechanisms beyond the effect. On the other hand, they can be used to assess the suitability of gate-tunable superconducting elements for applications such as superconducting logic or fast microwave switching.

In this Letter, we explore the dynamic properties of the field effect on a superconducting nanowire (Dayem) embedded in a $\lambda/4$ superconducting microwave resonator. We probe the system's dynamics by introducing a perturbation, specifically by applying a gate pulse to the superconducting Dayem, followed by the time-resolved measurement of the coherent scattering parameters of the resonators. Our study focuses on two distinct gate configurations and geometry: a finger gate placed within 70 nm of the Dayem bridge and a pair of remote electrodes. These electrodes are similarly spaced and positioned 1 μm away from the

Dayem bridge. Our findings identify distinct response time scales that are attributed to the varying mechanisms activated by each gate configuration. Direct quasiparticle injection in the vicinity of the gate or nanowire, dependent on gate polarity, creates hot spots. This process results in a slower switching due to extended times for quasiparticle diffusion, scattering, phonon emission, and recombination. In contrast, the phonon-mediated pair-breaking approach facilitated by remote gate electrodes demonstrates a significantly faster response, highlighting its effectiveness.

The architecture of our devices consists of a superconducting thin film of Nb, 20 nm in thickness, patterned into a quarter-wave coplanar waveguide (CPW) microwave resonator, and shunted to the ground with a 1.2 μm long and 120 nm wide nanowire made of the same material [Figs. 1(a)–1(c)]. Strategically positioning the nanowire at the resonator's current anti-node accentuates the effect of the inductance of the nanowire L_K^{NW} variation on f_r, while the placement at the voltage node minimizes coupling between the resonator and the gate electrode. The center conductor of the CPW resonator is gradually tapered into the nanowire section to avoid any current crowding effects caused by abrupt width variations.[12] The resonators are capacitively coupled to a feedline and probed with a coherent microwave tone. Additionally, a gate

electrode also in Nb [colored red in Figs. 1(a)–1(c)] is connected via a 50 Ω impedance matched CPW waveguide, allowing the application of both static and pulsed voltage V_G to the nanowire. Four resonators are connected to the same feedline using frequency-domain multiplexing: two with type-A gates and two with type-B gates. The steady-state resonant frequencies of the devices investigated here are 4.138 and 6.360 GHz for type-A, and 7.075 and 7.208 GHz for type-B, respectively.

This investigation employs two distinct gate geometries: a finger-type gate {referred to as type-A [Fig. 1(b)]},[13,14] and a remote-electrode gate {referred to as type-B [Fig. 1(c)]}.[4,9,11] The type-A gate is positioned with a 70 nm gap from the nanowire, while the type-B gate is spaced 70 nm apart from the ground plane and set at a distance of 1 μm from the nanowire, leading to different electric field distributions around the gates. In type-A gate, the electric field is confined between the gate electrode and the nanowire. In contrast in type-B, the electric field is largely confined between the gate electrode and the adjacent ground electrode, with minimal extension to the nanowire.[9] As a gate voltage is applied, L_{NW} is modified and, consequently, the resonator's resonant frequency f_r is shifted.[5] All the measurements are conducted at the base temperature ($T_{mx} \sim 15$ mK) of a dilution refrigerator.
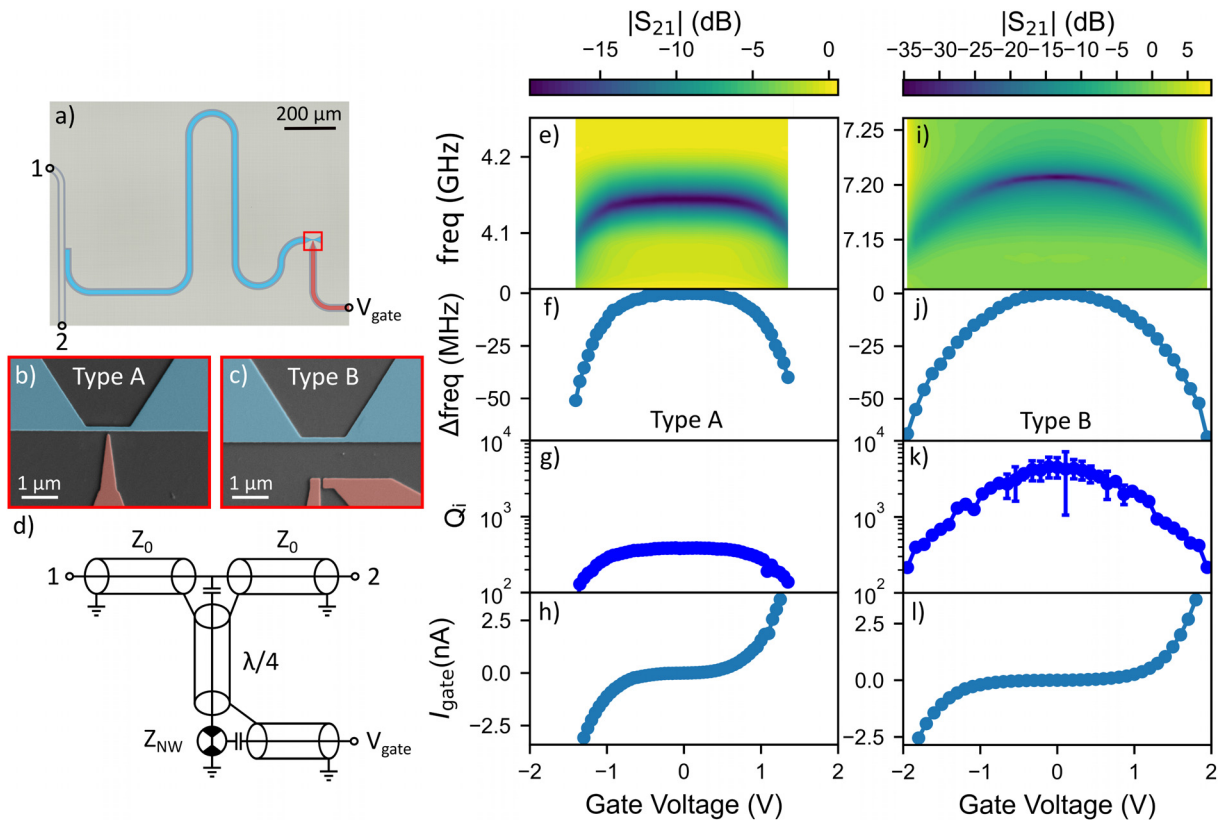
FIG. 1. Measured devices and CW measurements. (a) Optical image of one quarter-wave coplanar waveguide resonator capacitively coupled to a feedline (ports 1 and 2) and shunted to the ground through a 1.2 μm long NW. The scanning electron microscope (SEM) image of the NW shunt is shown in (b) with a finger-type gate (type-A) and with a remote gate in (c) (type-B). (d) Circuit diagram of a measured device. The transmission line resonator with impedance $Z_0 = 50 \Omega$ is shunted to ground by a NW with impedance Z_{NW}, which is gate controlled (V_{gate}), and capacitively coupled to the feedline with characteristic impedance Z_0. (e) Amplitude of the scattering parameter S_{21} in the function of the applied V_{gate} for type-A gate device. (f) and (g) Internal quality factor and frequency shift as a function of V_{gate} extracted from fits to S_{21} in (e). (h) Gate current I_{gate} as a function of V_{gate} simultaneously to the data in (e)–(g). (i) Amplitude of S_{21} for a device with type-B gate. We extract frequency shift (j) and the internal quality factor (k) from (i). (l) Gate leakage current measured simultaneously to the data in (i).

In Figs. 1(e) and 1(f), we plot the magnitude of complex transmission parameter $|S_{21}|$ vs gate voltage V_G, across f_r for two devices with type-A and type-B gate, respectively. By fitting the resonance traces[15] for each V_G, we extract the resonance frequencies (f_r) and internal quality factors (Q_i). We observe a monotonic decrease in both f_r [Figs. 1(f) and 1(j)] and Q_i [Figs. 1(g) and 1(k)] with increasing V_G. We note an increase in the leakage current I_{gate} with increasing V_G, and we limit our measurements to $|I_{gate}| \leq 2.5$ nA, thus $|1.2|$ V for type-A and $|2|$ V for type-B. This observed decrease in f_r can be attributed to an enhancement in the kinetic inductance of the nanowire (L_K^{NW}) due to a decrease in the superfluid density, which contributes to an augmented total inductance of the resonator.[16] Through electromagnetic (EM) simulations that model the nanowire as a lumped inductor while reflecting the precise device geometry of the distributed elements, we can predict the variation in f_r corresponding to changes in the nanowire's inductance. By comparing the EM simulations with measurements, we obtain a $\Delta L_K^{NW} = 16$ pH for max$|\Delta f_r|$ $= 50$ MHz for type-A gated, and very similar $\Delta L_K^{NW} = 14$ pH for max$|\Delta f_r| = 60$ MHz for type-B gated devices. We observe a distinct difference in the trends of V_G dependence on f_r and Q_i between the two device types. For type-A device, there is a gradual decline in f_r with increasing $|V_G|$, which accelerates once $|V_G| > 1$ V. A similar pattern is observed in Q_i also. Conversely, the type-B device demonstrates a consistent shift in both f_r and Q_i across the full $|V_G|$, exhibiting a near-parabolic dependence on $|V_G|$.

Furthermore, a strong correlation between the observed trends in f_r with the leakage current (supplementary material Fig. S3) suggests that the leakage current plays an important role in the voltage tunability of superconductivity.

After establishing the tunability of the resonances with V_G using spectroscopic measurements, we now probe the devices in time domain to quantitatively evaluate the performance of both gate geometries. This step is crucial for assessing their potential in constructing devices suited for practical applications.

We perform the following sequence of measurements. At $t = 0$, we apply a coherent tone of frequency f_p at the waveguide for a duration of total 100 μs. At the same time, starting at $t = 3$ μs, we apply a voltage pulse to the gate of fixed duration of 40 μs and varying amplitude [Fig. 2(a)]. We continuously record the complex amplitude of the coherently scattered signal through the feedline, with a sampling rate of 1 GS/s (see Methods). We note that by recording time traces at different probe frequencies f_p, we obtain more information than by examining the response at a single frequency or tracking the resonant frequency in response to V_{gate}. This approach allows us to examine the transient aspect of the resonator's response to the perturbation caused by the gate pulse, providing a deeper understanding of the dynamic processes at play. In the limit in which the nanowire dynamics is slower than the time constant of the resonator ($Q_L/2\pi f_r$), this time-resolved approach allows us to analyze both the resonator's time-dependent resonance frequency and its loaded quality factor Q_L, determined as the resonator width at the mid-height, showing how the system responds and recovers from the applied gate pulse.

We first examine the time-dependent scattering parameters of the type-A gate configuration, as shown in Figs. 2(b)–2(e). Specifically, line-cuts of S_{21} taken at two different time stamps, one prior and the other following the gate actuation [Fig. 2(d)] reveal a decrease in f_r, consistent with our earlier spectroscopic measurements (Fig. 1). In our initial analysis, we focus on the time trace of the resonance frequency at $V_G = 0$ V [Fig. 2(c)]. The time traces of $|S_{21}|$ near both the rise and fall edges is not described accurately by a single-exponential model. Instead, they necessitate a linear combination of two exponential functions in the form of $C_1 e^{-t/\tau_1} + C_2 e^{-t/\tau_2}$, where $\tau_{1,2}$ represent distinct characteristic time scales. For the initial rising part ($3 \leq t \leq 43$ μs) of the trace measured at $V_{gate} = 1.72$ V, a double-exponential fit unveils a short time constant ($\tau_{1,rise} = 450$ ns) followed by a longer one ($\tau_{2,rise} = 14$ μs). This indicates the presence of at least two kinetically distinct processes affecting the resonator's response. Analyzing line-cuts at nanosecond intervals yield real-time f_r (determined from the minima of $|S_{21}|$ vs f_p) and Q_L (determined from the full width at all maximum of $|S_{21}|$ at f_p). For Q_L [Fig. 2(e)], we observe an initial rapid decay over 450 ns, followed by a prolonged more gradual decline up to the fall edge of the gate pulse (at $t = 43$ μs). Similarly, $f_r(t)$ demonstrates a comparable bi-exponential behavior with an initial fast decay of $\tau_{1,rise} = 450$ ns before transitioning to a slower one with characteristic time $\tau_{2,rise} = 14.5$ μs.

At the gate pulse's end, the decrease in $|S_{21}|$ also follows a dual-exponential decay, characterized by a short time constant $\tau_{1,fall} = 470$ ns and a subsequent lengthier one $\tau_{2,fall} = 14.2$ μs. Additionally, f_r follows a corresponding recovery pattern. For Q_L, a similar rapid initial response is observed; however, its recovery to the initial steady-state is prolonged, extending up to 34 μs after the gate pulse ends, indicating that the kinetics governing the resonator's frequency shift (L_K^{NW}) operate more rapidly than those affecting its losses upon applying the gate voltage. For the type-B device [Figs. 2(f) and 2(i)], we observe a significantly faster resonator response to voltage pulses compared to type-A configuration. The time traces around both the rise and fall edges are best fit by single-exponential functions, with time constants of $\tau_{rise} = 27$ ns and $\tau_{fall} = 26$ ns [Fig. 2(g)]. This rapid response is uniform across both Q_L and f_r. For comparison, the resonant frequency and loaded quality factor of the type-B resonator give a characteristic time constant $Q_L/2\pi f_r = 25$ ns.

Upon analyzing the response to varying V_G for the type-A device [Figs. 3(a)–3(d)], the shorter response time, τ_1, remains largely constant for both rise and fall edges, suggesting a stable initial response of the resonator to the gate pulse. In contrast, the longer response time, τ_2, for the fall edge, monotonically increases with higher V_G values, implying that the mechanisms governing the superconductivity relaxation in the nanowire decelerate as the voltage amplitude increases. A contrasting behavior is observed with the type-B gate configuration, where time constants for both the rise and fall edges decrease with an increasing V_G [Figs. 3(e)–3(g)]. Notably, the time constant for the fall edge shows a more pronounced reduction. This phenomenon can be attributed to the quasiparticle recombination rate being inversely proportional to the quasiparticle density, implying that higher quasiparticle densities lead to faster recombination rates.[17] It is important to note that the measurement of the tuning speed, based on changes in the scattering parameters, is constrained by the ring-up time of the resonator, quantified by Q_L/ω_0. In our experiments, this duration is approximately 15 ns for the type-A device and 25 ns for type-B (supplementary material Fig. S4). This constraint suggests that observed tuning dynamics, particularly for type-B, are near the resonator's response limit, indicating potential for faster actuation not fully captured in our analysis.
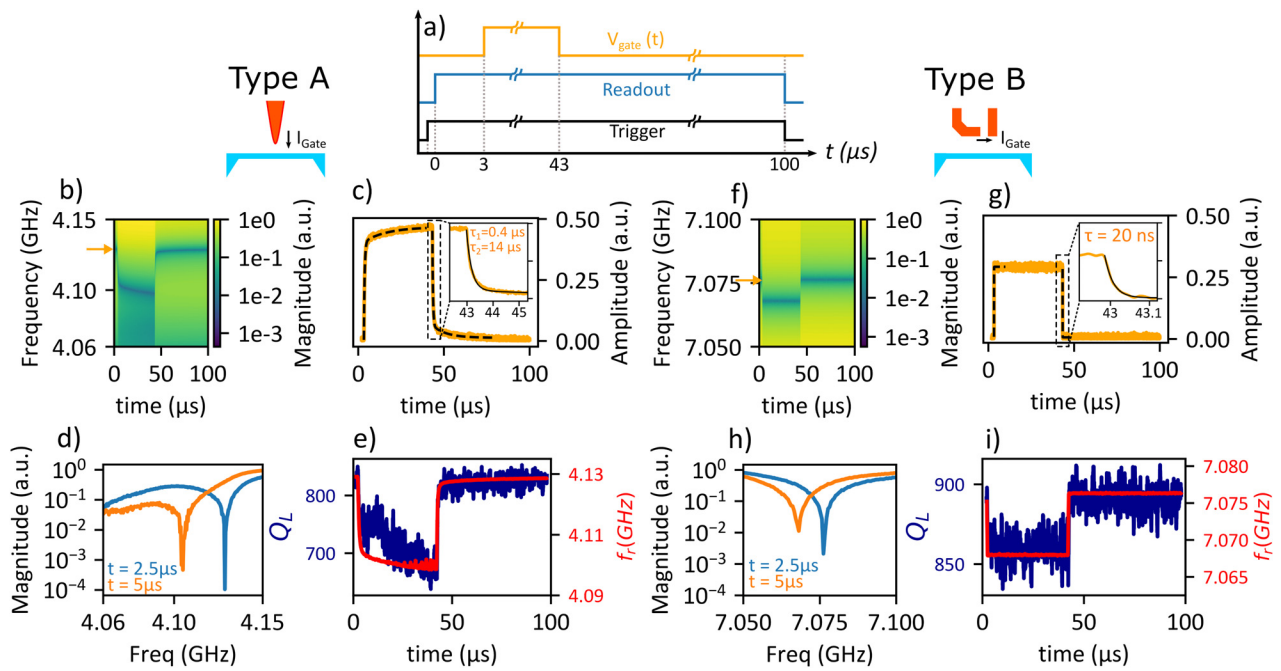
06 September 2024 12:10:58

FIG. 2. Time-domain characterization scattering parameters. (a) Pulse sequence of the measurement. Time trace showing the amplitude of S_{21} for the type-A device near the resonator frequency in (b) and type-B in (f). (c) and (g) Responses of the resonator to the gate pulse, measured at the steady-state resonance frequency (indicated by the orange arrow), for types-A and -B, respectively. The insets zoom in on the fall time. (d) and (h) line-cuts from the dataset in (b) and (f), respectively, taken at two specific time stamps (before and after the gate actuation), illustrating the magnitude of the resonator's S_{21}. (e) and (i) Loaded quality factor (blue curves), defined as $f_r/\delta f$, where δf is the full width at half maximum of the S_{21} magnitude dip and plotted along with the resonance frequency (red curves). The gate pulse amplitude used for (b) and (f) is 1.72 V.

To estimate how fast we can modulate the Dayem bridge in both gate configurations, we perform heterodyne measurements by mixing the signal leaking out from the modulated resonator at frequency f_{mod} with the drive signal f_r [Fig. 4(a)]. Put simply, the gate undergoes modulation at frequency f_{mod}, while we maintain a constant DC bias close to the onset gate threshold. The amplitude of the sidebands at the intermediate frequency (IF) $f_{IF} = |f_r - f_{mod}|$ [Fig. 4(b)], resulting from this mixing, is recorded and plotted as a function of f_{mod} [Fig. 4(c)]. The presence of sidebands in the spectra is indicative of a coherent process. In the type-A gate configuration, modulation sidebands were observed up to 120 MHz, corresponding to a modulation period of 8.3 ns, with the −3 dB cutoff at 12 MHz indicating the effective bandwidth of the system. As anticipated, the type-B gate exhibited a more rapid modulation capability, with a −3 dB cutoff at 37 MHz and modulation sidebands extending up to 500 MHz corresponding to a modulation period of 2 ns. We believe that the observed cutoff for type-B is limited by attenuation in the lossy coaxial cable used to drive the gate (see the supplementary material), suggesting that it could be possible to modulate the type-B device faster than reported. We observe that the sideband amplitude for the type-A gate is 18 dB weaker than that for the type-B gate, indicating a more efficient tuning mechanism associated with type-B.

In our study, we explored the dynamics properties of a Dayem bridge integrated within a microwave resonator, highlighting how gate geometry critically affects the speed at which an NW can be actuated with a voltage pulse. The traditional finger-type gate (type-A),[13,14] presents a slower switching response, with a limitation of around

~15 µs, making it less suitable for high-speed device application. Conversely, employing a set of remote electrodes positioned 1 µm away from the nanowire enhances the response speed, achieving modulation frequencies up to 500 MHz. This configuration stands out as the preferable configuration to develop advanced high-speed superconducting logic devices. The modulation of superconductivity by gate voltage in both types of devices is closely associated with the generation of leakage current.[18] However, the flow and the resultant impact of this current vary based on the gate configuration. In type-A devices, the process is influenced by the polarity of V_{gate}: when V_{gate} is negative, high-energy electrons are injected from the gate into the Dayem bridge, heating the nanowire. Conversely, a positive V_{gate} causes electron injection from the Dayem bridge into the gate, leading to gate heating. These quasiparticles, with energies roughly equal to eV_{gate} and significantly surpassing the superconducting gap of Nb,[19,20] generate hot spots within the superconductor. These hot spots reach equilibrium through recombination and diffusion processes,[17,21] affecting both the nanowire and the gate. Regardless of the gate voltage polarity, the electronic system of the superconductor experiences heating due to its interaction with a warmer phonon bath, leading to a non-equilibrium state in the quasiparticle system, effectively described by an elevated electronic temperature. It should be noted that although an asymmetry in resonator tunability is observed for the same gate amplitude with differing polarities, no asymmetries with gate polarities in the switching time scales were observed for the type-A gate configuration.

In contrast, the type-B gate configuration, characterized by an adjacent ground electrode and its relatively distant placement,
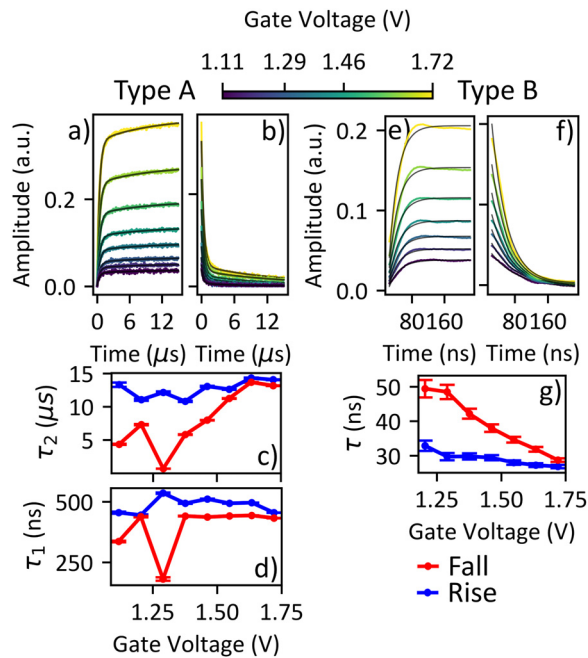
FIG. 3. Response time of the resonator's frequency relative to gate pulse amplitude. (a) and (b), Time-domain traces and fits of the resonator response ($|S_{21}|$) as a function of gate pulse amplitude for the type-A device with (a) showing the onset of the gate pulse (rise) and (b) showing the fall. The zero on the time axis corresponds to the start or the end of the gate pulse, respectively. (c) and (d) Rise (blue) and fall (red) time constants for the type-A gate: (c) slow response times and (d) fast response times for both rise and fall for type-A geometry. (e) and (f) Time traces for the type-B device. (g) Rise and fall time constants for the type-B gate.
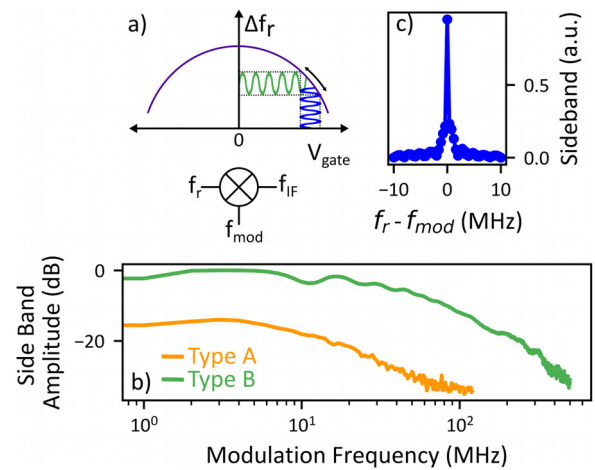

FIG. 4. Measurements of fast switching speeds conducted by mixing the signal from the resonator with the drive frequency, while a continuous wave (CW) tone and a constant DC bias are applied to the gate. (a) Schematic diagram of the heterodyne measurement setup. (b) Sideband amplitude as a function of the modulation frequency for type-A and type-B gates. The DC bias for each gate type is optimized to achieve maximum modulation speed. (c) Sideband spectrum centered at the intermediate frequency (IF).

effectively mitigates direct quasiparticle injection into the nanowire. Instead, this setup induces a phonon flux, originating from the remote gate electrodes through a process analogous to the hot-spot formation and quasiparticle recombination observed in the type-A configuration, although occurring from a distance. These phonons propagate through the substrate, breaking Cooper pairs within the nanowire.[22,23] The maximum energy carried by longitudinal acoustic phonons at the Brillouin zone boundary in Si is approximately 60 meV,[24] significantly lower than the energy of quasiparticles injected directly in the type-A scenario. This difference facilitates a quicker cascading from the pair-breaking phonons' energy to sub-gap quasiparticles. Consequently, superconductivity is restored as the quasiparticle density returns to its thermal equilibrium.[25] Given the lower energy of the charge carriers and their disparate decay locations in the type-B configuration, their heat release and overall impact on the device also differ.

The time scales observed in modulating the resonator's resonance frequency underscore the distinct impacts of phonon-mediated heating, which are influenced by the gate geometry. The presence of two time scales in type-A devices, significantly differing in magnitude, suggests the coexistence of multiple processes in modulating the resonances.[18] It is noteworthy that quasiparticle injection in the Dayem bridge, for types-A or -B, increases with the gate voltage's magnitude. However, the measured time scales diverge significantly between gate architecture: the type-A device's lower fall time scale, τ_2, increases with V_G, whereas the type-B device's fall time, τ, decreases with V_G. Further

experimental investigations could shed light on the complex interplay of mechanisms behind the voltage-induced superconductivity modulation.

Our findings offer an insight into the complex temporal dynamics within such devices, potentially paving the way for innovative superconducting electronic applications. The limited switching frequency of type-B devices, constrained by the thermo-coax's bandwidth used in our measurements, suggests room for improvement. By adopting on-chip filtering and measurement lines with broader bandwidths, we could potentially enhance the observable switching frequency threshold. Such rapid tunability of microwave resonances could lead to the development of on-chip superconducting microwave switches, offering minimized crosstalk, a common issue in flux-controlled devices. Our research lays the groundwork for advancing superconducting technologies through these innovative device architectures.

See the supplementary material for additional data on a second device featuring both gate types, along with an analysis of the response time as a function of readout power and temperature. Details on the fabrication process and experimental setup are provided. The supplementary material includes 2.5D electromagnetic simulations for estimating changes in the inductance of the Dayem bridge relative to the applied gate voltage and experimental data on frequency shifts in resonators as influenced by gate current leakage and gate power dissipation.

AUTHOR DECLARATIONS
Conflict of Interest

The authors have no conflicts to disclose.

Author Contributions

François Joint: Conceptualization (equal); Data curation (equal); Formal analysis (equal); Investigation (equal); Methodology (equal); Software (equal); Writing – original draft (equal); Writing – review & editing (equal). **Kazi Rafsanjani Amin:** Data curation (supporting); Investigation (equal); Methodology (equal); Software (equal); Writing – review & editing (equal). **Ivo P. C. Cools:** Data curation (supporting); Formal analysis (supporting); Methodology (supporting); Writing – review & editing (supporting). **Simone Gasparinetti:** Funding acquisition (equal); Project administration (equal); Supervision (equal); Writing – review & editing (equal).

DATA AVAILABILITY

The data that support the findings of this study are available from the corresponding author upon reasonable request.

REFERENCES

[1] R. Acharya, S. Brebels, A. Grill, J. Verjauw, T. Ivanov, D. P. Lozano, D. Wan, J. Van Damme, A. M. Vadiraj, M. Mongillo, B. Govoreanu, J. Craninckx, I. P. Radu, K. De Greve, G. Gielen, F. Catthoor, and A. Potočnik, Nat. Electron. **6**, 900–909 (2023).

[2] G. De Simoni, F. Paolucci, P. Solinas, E. Strambini, and F. Giazotto, Nat. Nanotechnol. **13**, 802–805 (2018).

[3] T. Elalaily, O. Kürtössy, Z. Scherübl, M. Berke, G. Fülöp, I. E. Lukács, T. Kanne, J. Nygård, K. Watanabe, T. Taniguchi, P. Makk, and S. Csonka, Nano Lett. **21**, 9684 (2021).

[4] M. F. Ritter, A. Fuhrer, D. Z. Haxell, S. Hart, P. Gumann, H. Riel, and F. Nichele, Nat. Commun. **12**, 1266 (2021).

[5] G. Catto, W. Liu, S. Kundu, V. Lahtinen, V. Vesterinen, and M. Möttönen, Sci. Rep. **12**, 6822 (2022).

[6] L. D. Alegria, C. G. L. Bøttcher, A. K. Saydjari, A. T. Pierce, S. H. Lee, S. P. Harvey, U. Vool, and A. Yacoby, Nat. Nanotechnol. **16**, 404 (2021).

[7] J. Basset, O. Stanisavljević, M. Kuzmanović, J. Gabelli, C. H. L. Quay, J. Estève, and M. Aprili, Phys. Rev. Res. **3**, 043169 (2021).

[8] I. Golokolenov, A. Guthrie, S. Kafanov, Y. A. Pashkin, and V. Tsepelin, Nat. Commun. **12**, 2747 (2021).

[9] M. F. Ritter, N. Crescini, D. Z. Haxell, M. Hinderling, H. Riel, C. Bruder, A. Fuhrer, and F. Nichele, Nat. Electron. **5**, 71 (2022).

[10] L. Ruf, T. Elalaily, C. Puglia, Y. P. Ivanov, F. Joint, M. Berke, A. Iorio, P. Makk, G. De Simoni, S. Gasparinetti, G. Divitini, S. Csonka, F. Giazotto, E. Scheer, and A. D. Bernardo, APL Mater. **11**, 091113 (2023).

[11] Y. Ryu, J. Jeong, J. Suh, J. Kim, H. Choi, and J. Cha, Nano Lett. **24**, 1223–1230 (2024).

[12] J. R. Clem and K. K. Berggren, Phys. Rev. B **84**, 174510 (2011).

[13] C. Puglia, G. De Simoni, and F. Giazotto, Materials **14**, 1243 (2021).

[14] J. Koch, C. Cirillo, S. Battisti, L. Ruf, Z. M. Kakhaki, A. Paghi, A. Gulian, S. Teknowijoyo, G. De Simoni, F. Giazotto, C. Attanasio, E. Scheer, and A. D. Bernardo, Nano Res. **17**, 6575–6581 (2024).

[15] S. Probst, F. B. Song, P. A. Bushev, A. V. Ustinov, and M. Weides, Rev. Sci. Instrum. **86**, 024706 (2015).

[16] L. J. Splitthoff, A. Bargerbos, L. Grünhaupt, M. Pita-Vidal, J. J. Wesdorp, Y. Liu, A. Kou, C. K. Andersen, and B. van Heck, Phys. Rev. Appl. **18**, 024074 (2022).

[17] C. M. Wilson, L. Frunzio, and D. E. Prober, Phys. Rev. Lett. **87**, 067004 (2001).

[18] T. Elalaily, M. Berke, I. Lilja, A. Savin, G. Fülöp, L. Kupás, T. Kanne, J. Nygård, P. Makk, P. Hakonen, and S. Csonka, "Switching dynamics in Al/InAs nanowire-based gate-controlled superconducting transistor," arXiv:2312.15453 (2023).

[19] A. N. McCaughan and K. K. Berggren, Nano Lett. **14**, 5748 (2014).

[20] A. N. McCaughan, V. B. Verma, S. M. Buckley, J. P. Allmaras, A. G. Kozorezov, A. N. Tait, S. W. Nam, and J. M. Shainline, Nat. Electron. **2**, 451 (2019).

[21] S. B. Kaplan, C. C. Chi, D. N. Langenberg, J. J. Chang, S. Jafarey, and D. J. Scalapino, Phys. Rev. B **14**, 4854 (1976).

[22] A. Semenov, A. Engel, H.-W. Hübers, K. Il'in, and M. Siegel, Eur. Phys. J. B **47**, 495 (2005).

[23] A. D. Semenov, G. N. Gol'tsman, and A. A. Korneev, Phys. C: Supercond. **351**, 349 (2001).

[24] P. Giannozzi, S. De Gironcoli, P. Pavone, and S. Baroni, Phys. Rev. B **43**, 7231 (1991).

[25] U. Patel, I. V. Pechenezhskiy, B. L. T. Plourde, M. G. Vavilov, and R. McDermott, Phys. Rev. B **96**, 220501 (2017).